Journal of Applied Mechanics and Technical Physics, Vol. 51, No. 2, pp. 233–240, 2010

AIR FLOW IN THE HUMAN NASAL CAVITY

V. M. Fomin,[1] **V. N. Vetlutsky,**[1,*]
V. L. Ganimedov,[1] **M. I. Muchnaya,**[1]
V. N. Shepelenko,[1] **M. N. Melnikov,**[2] **and A. A. Savina**[3]

UDC 533.6.011:51 + 612.215.4

A mathematical model of the air flow in the human nasal cavity is developed under the assumption of a turbulent viscous air flow. The shape of the nasal cavity is modeled with the use of the Gambit graphical software system and tomography data. A numerical solution is obtained by using the Fluent commercial software system. Calculations are performed for various variants of construction of the human nasal cavity.

Key words: *mathematical modeling, nasal cavity, skeleton model, coronary sections, mass flow, stagnant zones.*

1. The study of the air flow in the human nasal cavity is of significant interest because breathing is mainly performed through the nose. It is known that the human nose, like the nose of any animal, performs a number of important functions. When air passes through the nose during inhaling, it is humidified, heated in cold weather, cooled in hot weather, and partly cleaned from impurity particles suspended in air. In addition, the nose is an organ of smell, performs the reflectory and disinfecting functions, and perceives odorless substances–attractants, which are important for the emotional sphere of human activity. The nose can perform these functions owing to the complicated anatomical structure of the nasal cavity. The free area of the nose passage can be substantially changed owing to possible development of various pathological processes in the nasal cavity, which obstructs nasal breathing. As nasal breathing is a natural physiological process for humans, and violation of correct nasal breathing affects functioning of various systems in the human organism, it is important to ensure correct nasal breathing. Pharmacological means used for this purpose are often ineffective, and the problem has to be solved by surgery. Surgery interference, however, cannot always ensure a desired result, because the air flow in the nasal cavity has a complicated three-dimensional character, and the main flow may fail to pass through a correct nose passage. Moreover, a streamwise vortex may form in the flow, which increases the total drag of the nose passages, i.e., involves additional problems of breathing. Therefore, surgical expansion of nose passages should be performed with due allowance for the possibility of irreversible side effects.

Experimental investigations of the velocity field in the human nasal cavity is impossible, because probe insertion disturbs the flow. Optical methods are also inapplicable because of a significant curvature of the nose passage. Therefore, measurements performed on artificial models of the nasal cavity are used. A possible alternative to experiments is mathematical modeling, which makes it possible to study the real geometry of the nasal cavity and obtain full information about the flow, including the mass flow rate and the total drag of the nose passage. In addition, this approach allows virtual operations to be performed for predicting possible consequences of real surgical interference.

*Deceased.

[1]Khritianovich Institute of Theoretical and Applied Mechanics, Siberian Division, Russian Academy of Sciences, Novosibirsk 630090; ganim@itam.nsc.ru. [2]Institute of Traumatology and Orthopedy, Novosibirsk 630091. [3]Center of New Medical Technologies, Novosibirsk 630090. Translated from Prikladnaya Mekhanika i Tekhnicheskaya Fizika, Vol. 51, No. 2, pp. 107–115, March–April, 2010. Original article submitted June 1, 2009.

To study the flow in the nasal cavity, it is necessary to define the geometry of its inner surface, which has a rather complicated shape. Thus, in the nasal cavity cross sections perpendicular to the main flow direction, the surface can transform several times from the convex to the concave surface and vice versa; the curvature changes within wide limits; the number, shape, and size of side branches can also be different. (These reasons are partly responsible for the fact that a standard model of the human nasal cavity has not been developed yet.) The shape of the nasal cavity is defined on the basis of x-ray or magnetic resonance tomography data, which allows constructing a mathematical model of the nasal cavity of a particular person. For a fixed geometry of the nasal cavity, the flow calculations should be performed with the use of the three-dimensional Navier–Stokes equations, because both flow three-dimensionality and viscous effects are important factors.

2. Calculations of the flow in the human nasal cavity with modeling its shape on the basis of tomography data and with the use of an ideal gas model were started back in the 1990s. Before discussing the main results obtained so far, let us briefly explain terms used in rhinology. Figure 1 shows the coronary sections of the nasal cavity, which are approximately orthogonal to the hard palate and to the main flow direction in the nasal cavity. The nasal cavity is a variable-section duct communicating with the ambient medium through the nose orifices in the front and with the nasal pharynx in the back. The nasal cavity is divided by the nasal septum into the left and right parts. The nasal cavity walls opposite to the nasal septum contain almost horizontal and almost parallel bone projections covered with a mucus membrane: nose conchas (the upper, middle, and lower conchas, and the upper concha is not necessarily present). The spaces bounded by the side nose wall and these conchas are called the nose passages (correspondingly, the upper, middle, and lower nose passages). The space between the nose septum and the side surface of the nose conchas is called the common nose passage. In addition to coronary sections, we also consider sagittal sections parallel to the mid-plane of the human body.

One of the first calculations of the laminar flow in the nasal cavity of a healthy grown-up person was performed in [1]. It was found that the maximum velocity during inhaling was reached in the lower part of the nose passage, and the second velocity peak was observed in the middle part of the common passage. The mass flow of air through the lower part of the nasal cavity was approximately 30% of the total mass flow of air, and the mass flow through the olfactory tracts (upper narrow part of the common passage) was approximately 10% of the total mass flow. Weak secondary flows were observed. The flow pattern changes insignificantly in the air mass flow range $Q = 125$–200 ml/sec. The velocity maximums during breathing-out are lower than in the case of breathing-in, and the air flow is more uniform in the region of nasal conchas. A comparison of the calculated results with experimental data obtained for the nose model scaled $20:1$ showed their good agreement. Keyhani et al. [1] concluded that the flow in the nasal cavity is laminar during quiet breathing.

Hörschler et al. [2] started a series of numerical and experimental investigations of flows in artificial schematic models of the nasal cavity to study the influence of various parts of the nasal cavity on the flow pattern. Hörschler et al. [3] reported results for models with and without side branches, with and without projections on the nasal septum. The results were obtained for the air mass flow values $Q = 159$ and 127 ml/sec, which corresponds to the Reynolds numbers based on the flow parameters in the throat $\mathrm{Re} = 500$ and 400. The calculations were performed on an irregular difference grid with the number of nodes up to 250,000. The flow pattern in several sagittal planes and the streamlines of air in the entire nasal cavity were presented. It was shown that the calculated results are in good qualitative agreement with experimental data obtained in a model with 1.5-fold magnification. It was also demonstrated that the flow is most sensitive to changes in the nasal concha shape during inhaling, and the nasal conchas promote a uniform velocity distribution in the lower, middle, and upper passages between the nostrils and the throat. The nasal cavity configurations studied in [4] had different sizes of the nasal valve (the smallest cross section at the beginning of the nose passage) and different shapes of the lower nose passage; different combinations of these parameters were studied. The Reynolds number based on the throat diameter was $\mathrm{Re} = 1170$. It was found that the pressure inside the nasal cavity can be controlled by changing the cross-sectional area of the nasal valve, whereas a decrease in the lower nose passage width can reduce the air mass flow through the nasal cavity.

Kelly et al. [5] used the particle image velocimetry (PIV, an optical method of measuring the fluid velocity fields in a chosen cross section of the flow) to measure the velocity distributions in a nasal cavity model constructed with twofold magnification on the basis of 26 pictures taken with computer tomography. They concluded that the flow was laminar at the air mass flow $Q = 125$ ml/sec and turbulent at $Q = 200$ ml/sec. The maximum flow velocity was registered in the lower part of the nose passage. A comparatively weak flow takes place in the

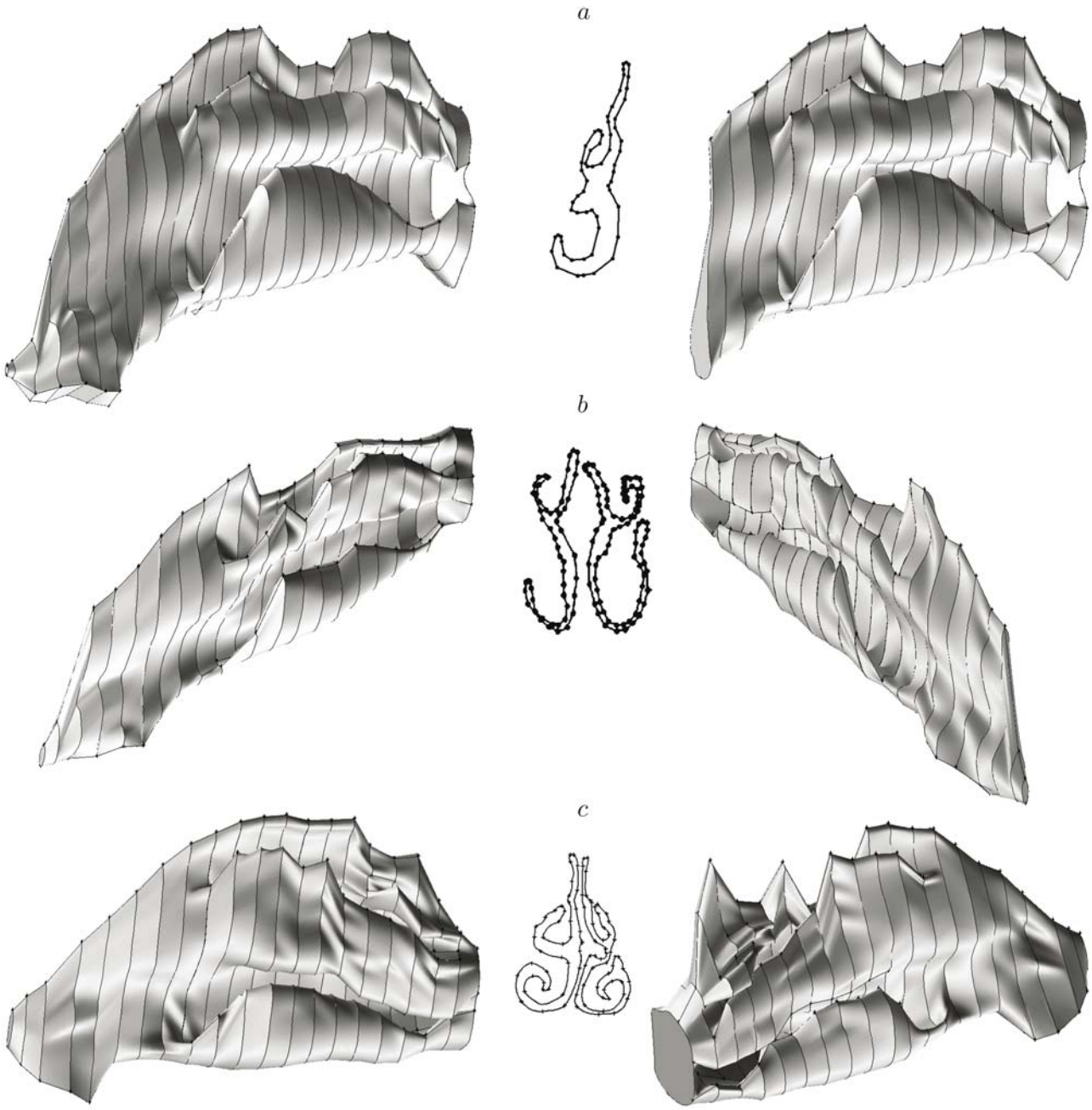

Fig. 1. Possible nose passages (side view): (a) variant No. 1, physiologically normal left nose passage (the full and truncated views are shown on the left and on the right, respectively); (b) variant No. 2, left and right nose passages with pathological changes, but with non-obstructed breathing; (c) variant No. 3, left and right nose passages with pathological changes and with obstructed breathing; the figures in the middle show the coronary sections of the nasal cavity.

upper olfactory slot. Low velocities were also observed in the upper nose passage. A comparison of consecutive frames allowed a conclusion of a steady flow to be drawn. Kelly et al. [5] reviewed investigations performed for air mass flows $Q \leqslant 250$ ml/sec, but those studies were carried out with different nasal cavity models, which hinders quantitative comparisons of results.

Garcia et al. [6] studied a gas flow in the nasal cavity with allowance for heat conduction both theoretically and experimentally. They considered a steady flow with the air mass flow $Q = 250$ ml/sec for the inhaled air temperature of 20°C and humidity of 50%. The calculations showed that the nose heated the air to a temperature of 32.6°C. Calculations for two-phase flows with aerosol particles of different diameters were also performed. It was found that particles greater than 10 μm in diameter were usually deposited in the nasal cavity, whereas smaller particles flew farther. It was noted that the particle deposition process also depends on the velocity of aerosol injection.

3. In the present work, the shapes of the right and left nose passages were modeled on the basis of a series of tomograms in parallel coronary sections, which were obtained by an x-ray tomograph with a step of 4 mm. The coordinates of the image of the nose passage contour were converted from the analog to the discrete (digital) form in the Grapher standard software system. After that, a skeleton model was constructed in the Gambit geometry pre-processor of the Fluent commercial software system on the basis of the point coordinates. Each contour in a particular cross section was reconstructed with the use of NURBS-splines. After that, the surface modeling the nose passage walls was "pulled up" onto these "frames." Then, the shape of the computational domain was modeled in the Gambit pre-processor, and irregular volume difference grids with a specified cell size were constructed.

A steady air flow in nose passages in the breathing-in and breathing-out regimes was calculated in the Siberian Supercomputer Center of the Siberian Division of the Russian Academy of Sciences with the use of the Fluent software system. A left-hand rectangular coordinate system with the Z axis directed from the nose entrance perpendicular to the coronary sections and the Y axis directed vertically upward was used in the computations. Incompressible Navier–Stokes equations were used to describe the flow. As large pressure differences were set in the computations, the flow was assumed to be turbulent. The turbulence was described by the k–ω model suitable for calculating near-wall flows [7]:

$$\frac{\partial u_j}{\partial x_j} = 0, \qquad \rho\,\frac{\partial u_i}{\partial t} + \rho\,\frac{\partial\,(u_j u_i)}{\partial x_j} = -\frac{\partial p}{\partial x_i} + \frac{\partial \hat{\tau}_{ji}}{\partial x_j},$$

$$\rho\,\frac{\partial k}{\partial t} + \rho\,\frac{\partial\,(u_j k)}{\partial x_j} = \tau_{ij}\,\frac{\partial u_i}{\partial x_j} - \beta^*\rho\omega k + \frac{\partial}{\partial x_j}\Big((\mu + \sigma^*\mu_T)\,\frac{\partial k}{\partial x_j}\Big), \tag{1}$$

$$\rho\,\frac{\partial \omega}{\partial t} + \rho\,\frac{\partial\,(u_j \omega)}{\partial x_j} = \frac{\gamma\omega}{k}\,\tau_{ij}\,\frac{\partial u_i}{\partial x_j} - \beta\rho\omega^2 + \frac{\partial}{\partial x_j}\Big((\mu + \sigma\mu_T)\,\frac{\partial \omega}{\partial x_j}\Big).$$

In system (1) consisting of the continuity and momentum equations, and also equations for the energy of turbulent mixing k and specific dissipation rate ω, t is the time, x_i are the point coordinates in space, u_i are the mean velocity components, ρ is the density, p is the pressure, μ is the molecular viscosity, $\hat{\tau}_{ij}$ are the components of the sum of the molecular and Reynolds stresses, k is the energy of turbulent mixing, ω is the specific dissipation rate, $\mu_T = \gamma^*\rho k/\omega$ is the turbulent viscosity, and β, β^*, γ, γ^*, σ, and σ^* are the model coefficients. The total tensor of viscous stresses is calculated by the formula

$$\hat{\tau}_{ji} = 2\mu\Big(S_{ij} - \frac{1}{3}\,\frac{\partial u_k}{\partial x_k}\delta_{ij}\Big) + \tau_{ij},$$

where S_{ij} is the tensor of the mean strain rates:

$$S_{ij} = \frac{1}{2}\Big(\frac{\partial u_i}{\partial x_j} + \frac{\partial u_j}{\partial x_i}\Big).$$

The tensor of the Reynolds stresses is proportional to the tensor of the mean strain rates:

$$\tau_{ij} = 2\mu_T\Big(S_{ij} - \frac{1}{3}\,\frac{\partial u_k}{\partial x_k}\,\delta_{ij}\Big) - \frac{2}{3}\,\rho k\delta_{ij}.$$

The no-slip conditions were imposed on the duct walls. A pressure difference between the duct entrance and exit was specified in the exit section; the value was negative in the case of inhaling and positive in the case of breathing-out. The computations were performed by a time-dependent method, and the error was taken to be 10^{-4}.

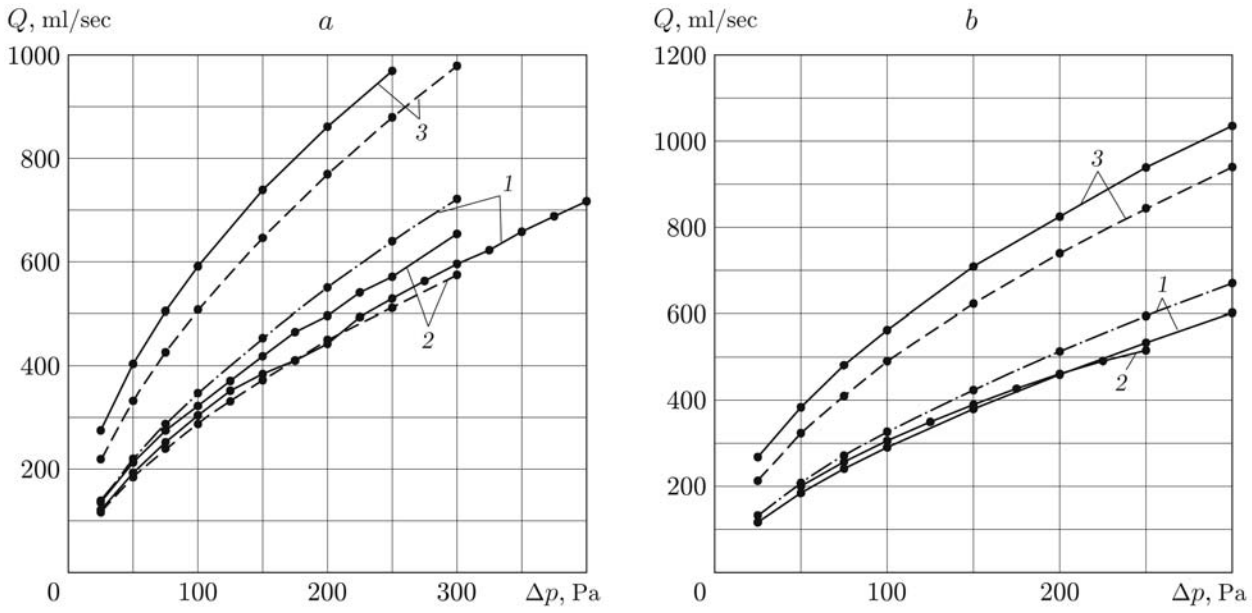

Fig. 2. Mass flow or air during breathing-in (1) and breathing-out (b) versus the pressure difference for different variants of nose passages shown in Fig. 1: curves 1–3 refer to variant Nos. 1–3, respectively; the solid and dashed curves show the results for the left and right nose passages, respectively; the dot-and-dashed curves refer to the truncated left nose passage for variant No. 1.

The basic results were obtained on grids with the number of volume cells equal to $(1.5–2.0) \cdot 10^6$. Some check-up computations were performed on a grid with the number of cells approximately equal to $3 \cdot 10^6$.

The computations give an idea about the distribution of the flow velocity vector at all points of the nasal cavity and allow determining the regions with the maximum velocity, stagnant zones where the flow velocity is close to zero, and reverse flow regions where the flow velocity is opposite to the main flow direction. Detection of these zones is rather important, because partial choking of the duct may occur, which leads to obstruction of nasal breathing. In addition, the air mass flow was calculated for each value of the pressure difference.

4. Various variants of the right and left nose passages of three patients were considered. These variants are illustrated in Fig. 1. Variant No. 1 (see Fig. 1a) corresponds to the physiological norm. In variant No. 2 (see Fig. 1b), some pathological changes in the nose passage shape were detected by means of clinical control, but the patient did not complain that he had any respiratory difficulties because the pathological changes were compensated by internal resources of the organism. Variant No. 3 (see Fig. 1c) was characterized by doctors as a pathological situation, i.e., the patient declared that he had problems with breathing. For variant No. 1, Fig. 1 shows the left nose passage as a full view (from the nostrils to the throat entrance) and as a truncated view (without the nostrils); for variant Nos. 2 and 3, Fig. 1 shows the right and left nasal cavities. The first calculations were performed for the truncated variant No. 1 (see Fig. 1a). It is shown below that the initial segment exerts a significant effect on the flow in the nasal cavity. For all variants, Fig. 1 also shows one coronary section approximately in the middle of the nose passage. These contours clearly show the common nose passage, the lower and middle nose passages, and the nose conchas between them. Figure 1c clearly shows an anomaly in the right half of the nasal cavity: a spike (projection) on the nasal septum, which partly blocks the flow. It is seen that the geometric parameters of the cases considered are essentially different, and the left and right nose passages in one variant are far from being symmetric. The calculations were performed in the breathing-in and breathing-out regimes with the pressure difference $\Delta p = 50–300$ Pa (the values $\Delta p = 300$ Pa and $\Delta p = 150$ Pa correspond to deep and quiet breathing, respectively).

Figure 2a shows the mass flow of air as a function of the pressure difference during inhaling for three variants shown in Fig. 1 (the curves are constructed along the reference points). It is seen in Fig. 2a that the difference in air mass flows through the left and right nose passages owing to asymmetry of the nose passages of the patient can reach 10%. The difference in the mass flows for the full and truncated nose passages is approximately 20%, which

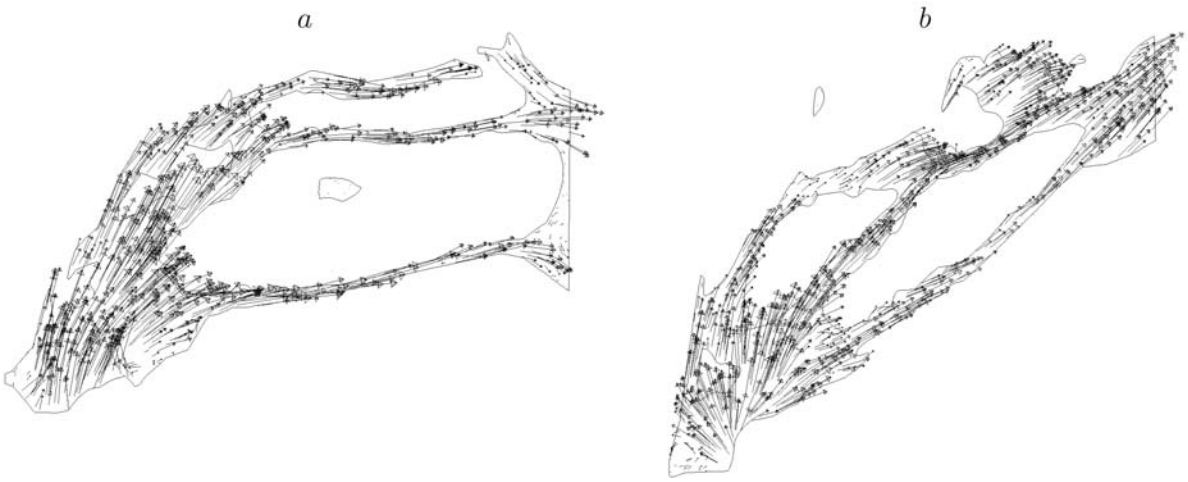

Fig. 3. Projections of the velocity vector onto the sagittal plane ($X = \text{const}$) in the inhaling regime for the left nose passage at $\Delta p = 150$ Pa for variant No. 1 (a) and variant No. 2 (b).

is caused by large pressure losses at the initial segment. The curves for variant Nos. 1 and 2 are close to each other, whereas the curves for variant No. 3 lie substantially higher, because the air mass flow in variant No. 3 is greater than that in variant No. 2 by a factor of 1.7. The volumes of the left nose passages for these three variants are $0.78 \cdot 10^{-5}$, $1.05 \cdot 10^{-5}$, and $1.65 \cdot 10^{-5}$ m^3, respectively, i.e., variant No. 3 refers to a patient with more developed nose passages whose volume is more than twice the volume of the nose passages for variant No. 1. Similar features are observed in Fig. 2b, which shows the air mass flow as a function of the pressure difference for the breathing-out regime. The curve corresponding to the right passage in variant No. 2 almost coincides with the same curve for variant No. 1. The air mass flows for the left and right nose passages in variant No. 2 are also close to each other. The difference in mass flows for the full and truncated nose passages in variant No. 1 is slightly greater than 10%. The air mass flow in variant No. 3 in the breathing-out regime is also greater than that in variant No. 2 by a factor of 1.7.

Figure 3a shows the projections of the velocity vector onto the sagittal plane ($X = \text{const}$) for the left nose passage in variant No. 1 during inhaling with $\Delta p = 150$ Pa, which corresponds to quiet breathing. Hereinafter, the length of the vectors is proportional to the absolute value of velocity. The flow pattern in Fig. 3a is typical for the normal (from the medical viewpoint) nose passage with the main air flow passing in the lower part. There is a moderate-size region of reverse flows in the frontal zone behind the nostril. The vortex formed here plays an important role in heat exchange. As the pressure difference increases, which corresponds to deeper breathing, the vortex in the input part of the nose becomes more intense. Figure 3b shows a similar flow pattern for the left nose passage in variant No. 2 for the same value of Δp. The flow considered here differs from the flow in variant No. 1 because the main flow passes over the middle part of the nose passage. The reverse flow region at the nose entrance is more extended, which is expected to cause some difficulties in breathing. This is not the case, however, and the air mass flow almost coincides with the mass flow for variant No. 1, because the nasal cavity volume here is greater by 30%. A similar flow pattern is observed for the right nose passage.

Figures 4a and 4b show the velocity distributions for the right nose passage in variant No. 3 during inhaling with the pressure difference $\Delta p = 300$ Pa. The fields of the streamwise velocity component in coronary sections are plotted in Fig. 4a. It is seen that the main nose passage is curves and constricted. Figure 4b shows the projections of the velocity vector onto the sagittal plane $X = \text{const}$. The main flow moves over the middle and right parts of the nose passage. Stagnant zones and moderate-size reverse flow regions are observed. Figures 4c and 4d show similar distributions for the left nose passage. In this case, there are no visible anomalies. Almost the entire lower nose passage, however, is the reverse flow region. The air mass flow in the left passage is greater than the air mass flow in the right (pathologically changed) nose passage (see Fig. 2a). Note that vast reverse flow regions did not appear in variant Nos. 1 and 2.

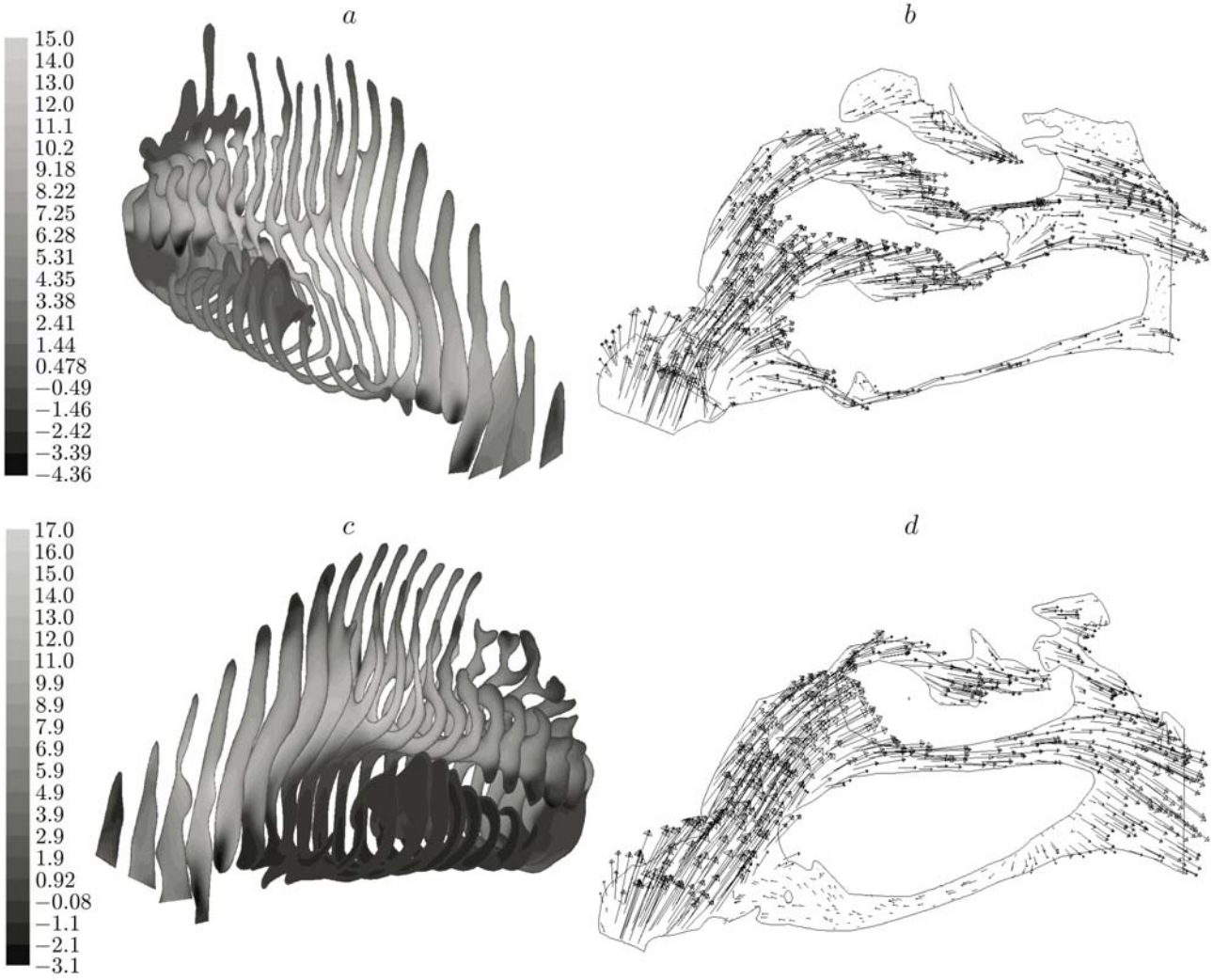

Fig. 4. Velocity distributions for the right (a and b) and left (c and d) nose passages in variant No. 3 during inhaling with $\Delta p = 300$ Pa: fields of the streamwise component of velocity in coronary sections (a and c); projections of the velocity vector onto the sagittal plane (b and d).

In the inhaling regime with the pressure difference $\Delta p = 150$ Pa, the maximum values of the streamwise velocity component are $V_z = 11$, 8, and 12 m/sec; for $\Delta p = 300$ Pa, we have $V_z = 20$, 13, and 18 m/sec, respectively. The negative values of the component V_z reach -9 m/sec in variant No. 1, -7 m/sec in variant No. 2, and $V_z = -15$ m/sec at $\Delta p = 150$ Pa and $V_z = -22$ m/sec at $\Delta p = 300$ Pa in variant No. 3. These maximum values are observed in the vicinity of the nose entrance. In the reverse flow region in the lower left nose passage in variant No. 3, we have $V_z = -2.5$ m/sec.

5. A mathematical technology of processing clinical rhinology objects was developed. The shapes of the nose passages were modeled with the use of tomograms and commercial codes, and irregular spatial finite-difference grids were constructed. The steady flow computations were performed on an Itanium2 supercomputer at the Siberian Supercomputer Center of the Siberian Division of the Russian Academy of Sciences with the use of the Fluent commercial software system and also with the Navier–Stokes model of the flow. Parametric computations of the flow in the nose passages in the breathing-in and breathing-out regimes were performed for three variants, one of them being characterized as pathological. The mass flow of air was plotted as a function of the difference in pressures at the duct entrance and exit. It was demonstrated that the losses in the input part of the nose passage, where the flow turning occurs, are fairly significant. Breathing-in flow patterns in coronary and sagittal sections

were obtained. The main air flow was found to pass through the lower (widest) part in physiologically normal nose passages and through the lower and middle parts in nose passages with pathological changes that do not involve breathing difficulties. In the case of pathological changes accompanied by breathing difficulties, the flow in the nose passages becomes cardinally different: the main air flow passes through the middle and upper parts, a stagnant zone is formed in the lower part in the right passage, and a vast reverse flow region is formed in the left passage.

Thus, the computations revealed significant differences in the flow fields in the nasal cavities considered. An analysis of the numerical results made it possible to identify the reasons for breathing obstructions. The examples considered show that the human nasal duct is unique and asymmetric. At the moment, it seems problematic to obtain universal standard dependences of the flow parameters on the nasal cavity shape.

REFERENCES

1. K. Keyhani, P. W. Scherer, and M. M. Mozell, "Numerical simulation of airflow in the human nasal cavity," *J. Biomech. Eng.*, **117**, 429–441 (1995).
2. I. Hörschler, M. Meinke, and W. Schröder, "Numerical simulation of the flow field in a model of the nasal cavity," *Comput. Fluids*, **32**, No. 1, 39–45 (2003).
3. I. Hörschler, Ch. Brücker, W. Schröder, and M. Meinke, "Investigation of the impact of the geometry on the nose flow," *Europ. J. Mech. B. Fluids*, **25**, No. 4, 471–490 (2006).
4. I. Hörschler, W. Schröder, and M. Meinke, "Numerical analysis of the impact of the nose geometry on the flow structure. 2. Nasal valve and lower turbinate," *Comput. Fluid Dyn. J.*, **16**, 243–260 (2008).
5. J. T. Kelly, A. K. Prasad, and A. S. Wexler, "Detailed flow patterns in the nasal cavity," *J. Appl. Physiol.*, **89**, 323–337 (2000).
6. J. M. Garcia, J. D. Schroeter, amd J. S. Kimbell, "Sniffing out airflow and transport processes in the nasal cavity," *Fluent News Appl. Comput. Fluid Dyn.*, **15**, iss. 3, 3–5 (2006).
7. D. C. Wilcox, "Reassessment of the scale determining equation for advanced turbulence models," *AIAA J.*, **32**, No. 11, 1299–1310 (1988).